Original Article

Effect of contrast material injection protocol on first-pass myocardial perfusion assessed by dual-energy dual-layer computed tomography

Sara Boccalini[1,2#^], Salim Si-Mohamed[1,3#], Maxime Matzuzzi[4], Manon Tillier[4], David C. Rotzinger[5], Didier Revel[1,3], Loic Boussel[1,3], Philippe Douek[1,3]

[1]Department of Cardiovascular and Thoracic Radiology, Hospices Civils de Lyon, Lyon, France; [2]Univerisity Claude Bernard Lyon 1, Lyon, France; [3]University Claude Bernard Lyon 1, CREATIS, CNRS UMR 5220, INSERM U1206, INSA-Lyon, France; [4]Faculty of Medicine Rockfeller, University Claude Bernard Lyon 1, Lyon, France; [5]Department of Radiology, University Hospital Center Vaudois, Lausanne, Switzerland

Contributions: (I) Conception and design: S Boccalini, S Si-Mohamed, DC Rotzinger, P Douek; (II) Administrative support: P Douek, L Boussel; (III) Provision of study materials or patients: S Boccalini, S Si-Mohamed, D Revel, P Douek; (IV) Collection and assembly of data: S Boccalini, S Si-Mohamed, M Matzuzzi, M Tillier; (V) Data analysis and interpretation: S Boccalini, S Si-Mohamed, DC Rotzinger, P Douek; (VI) Manuscript writing: All authors; (VII) Final approval of manuscript: All authors.

[#]These authors contributed equally to this work.

Correspondence to: Sara Boccalini, MD, PhD. Department of Cardiovascular and Thoracic Radiology, Hôpital Louis Pradel - Hospices Civils de Lyon, 28 Avenue de Doyen Lépine, 69500 Bron, Lyon, France. Email: sara.boccalini@chu-lyon.fr.

Background: Dual-energy dual-layer computed tomography (CT) scanners can provide useful tools, such as iodine maps and virtual monochromatic images (VMI), for the evaluation of myocardial perfusion defects. Data about the influence of acquisition protocols and normal values are still lacking.

Methods: Clinically indicated coronary CT-angiographies performed between January-October 2018 in a single university hospital with dual-energy dual-layer CT (DE-DLCT) and different injection protocols were retrospectively evaluated. The two protocols were: 35 mL in patients <80 kg and 0.5 mL/kg in patients >80 kg at 2.5 mL/sec (group A) or double contrast dose at 5 mL/sec (group B). Patients with coronary stenosis >50% were excluded. Regions of interest were manually drawn on 16 myocardial segments and iodine concentration was measured in mg/mL. Signal-to-noise, contrast-to-noise ratios (CNR) and image noise were measured on conventional images and VMI.

Results: A total of 30 patients were included for each protocol. With iodine concentrations of 1.38±0.41 mg/mL for protocol A and 2.07±0.73 mg/mL for protocol B, the two groups were significantly different (P<0.001). No significant iodine concentration differences were found between the 16 segments (P=0.47 and P=0.09 for group A and B respectively), between basal, mid and apical segments for group A and B (P=0.28 and P=0.12 for group A and B respectively) and between wall regions for group A (P=0.06 on normalised data). In group B, iodine concentration was significantly different between three wall regions [highest values for the lateral wall, median =2.03 (1.06) mg/mL]. Post-hoc analysis showed highest contrast-to-noise and signal-to-noise in VMI at 40 eV (P<0.05).

Conclusions: Iodine concentration in left ventricular myocardium of patients without significant coronary artery stenosis varied depending on the injection protocol and appeared more heterogeneous in different wall regions at faster injection rate and greater iodine load. Signal-to-noise and contrast-to-noise gradually improved when decreasing VMI energy, although at the expenses of higher noise, demonstrating the

^ ORCID: 0000-0002-1829-5834.

potential of DE-DLCT to enhance objective image quality.

Keywords: Computed tomography angiography (CT angiography); myocardial perfusion imaging; dual-energy computed tomography (DECT); iodine determination; image enhancement

Submitted Aug 15, 2021. Accepted for publication Mar 09, 2022.
doi: 10.21037/qims-21-809
View this article at: https://dx.doi.org/10.21037/qims-21-809

Introduction

Coronary computed tomography (CT) angiography is the standard non-invasive diagnostic technique for the anatomic detection of coronary stenosis. However, in the case of intermediate stenosis, it is difficult to determine whether it results in a perfusion defect. In fact, the presence of a coronary stenosis is not necessarily related to an impairment of myocardial blood flow that, on the contrary, is the factor guiding clinical management of patients with coronary artery disease (1,2). In recent years, multiple CT protocols have been proposed to assess, in a single diagnostic test, not only coronary artery anatomy but also myocardial perfusion under stress and at rest (3,4).

Dual-energy computed tomography (DECT) has been proposed to assess myocardial ischemia. Currently, several DECT methods are available based on the source (dual source, fast kilovoltage switching, double rotation and split beam) or detector (dual-layer) (5,6). With DECT, in addition to conventional images, virtual monochromatic images (VMI) and iodine maps can be derived. Due to its specific technology, dual-energy dual-layer CT (DE-DLCT) presents several features of interest for its feasibility and broad applicability in clinical practice. These include the possibility to perform an examination with standard parameters that does not need to be chosen beforehand, without any loss of temporal resolution and without temporal or spatial misalignment (7).

Separating low and high energy X-ray photons, DECT increases tissue contrast and enhances iodine attenuation (8). Low energy VMI have been shown to improve vascular contrast enhancement and therefore could facilitate the detection of perfusion defect. Moreover, monochromatic images could help reduce beam hardening artifacts (7,9).

To date, the evaluation of static first-pass perfusion images with conventional CT and DECT is performed qualitatively by visual assessment of alterations in myocardial density or iodine maps (10-12). However, quantification of iodine density could provide a more objective assessment and has been regarded to as a surrogate biomarker for myocardial perfusion. Only a few studies investigated myocardial iodine concentration in the attempt to establish cut-off values to distinguish healthy, ischemic and necrotic segments (13,14). Moreover, for DE-DLCT, although a few phantom studies have demonstrated the accuracy of iodine concentration measurements (15-17), there are no clinical data about such analysis in human myocardium. In addition, to the best of our knowledge, there are no data available regarding the effect of CT acquisition parameters on iodine concentration such as contrast material injection protocols.

Therefore, the purpose of this study was twofold: (I) to demonstrate the effect of contrast material injection rate on the iodine distribution during first-pass perfusion in the myocardium of patient without significant coronary artery stenosis; (II) to evaluate the impact of VMI on image noise, signal-to-noise ratio (SNR) and contrast-to-noise ratio (CNR). We present the following article in accordance with the STROBE reporting checklist (available at https://qims.amegroups.com/article/view/10.21037/qims-21-809/rc).

Methods

Study design

This was a single-centre, retrospective observational analysis carried out in a tertiary care, university hospital (Hôpital Louis Pradel, Hospices Civils de Lyon, Lyon, France). The study was conducted in accordance with the Declaration of Helsinki (as revised in 2013). The study was approved by the local ethics committee (No. 19-382) and informed consent was waived due to the retrospective nature of the study.

Population

Consecutive coronary-CTA scans performed from January to October 2018 in the clinical practice of a single tertiary care, university hospital with a DE-DLCT were

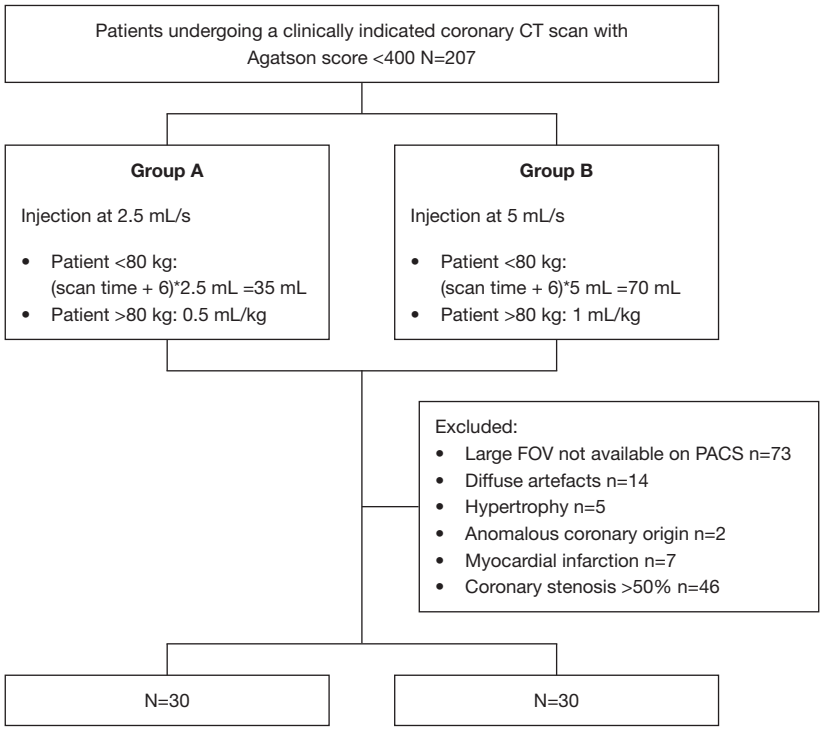

Figure 1 Flow-chart of the study. CT, computed tomography; FOV, field-of-view; PACS, picture archiving and communication system.

retrospectively included. The entirety of this population has been the object of coronary artery image quality assessment (18). All subjects underwent a preliminary non-contrast acquisition to calculate the calcium score and only those with an Agatson score <400 were further evaluated (N=207).

Subjects with coronary artery stenosis >50% (N=46), history or CT finding of myocardial infarction (N=7), anomalous malignant origin of coronary arteries (N=2) and myocardial hypertrophy (myocardial thickness >15 mm; N=5) were excluded from the analysis. Also CT scans with artefacts impeding the analysis of most segments (N=14) and those for which no reconstruction dedicated to myocardium analysis could be retrieved from the picture archiving and communication system (PACS) (N=73) were excluded (*Figure 1*).

Contrast material injection

Iomeprol 400 mg Iode/mL (Iomeron®; Bracco, Milan, Italy) was the only contrast material employed; it was heated before use and injected using a double head power injector.

Each patient underwent either a reduced flow protocol (2.5 mL/s rate, indicated as group A for the purpose of this study) or a standard injection protocol (5 mL/s rate, indicated as group B for the purpose of this study) depending on the quality of the venous access, as clinically established by the radiologist and paramedical personnel at time of the CT exam. The time of injection was constant between the two groups and contras media volume calculated accordingly.

For group A patients, the contrast material was administered into an 18G catheter, with a flow rate reduced to 2.5 mL/s (iodine rate =1 g/s) and followed by a 20 mL saline rinse at the same rate. The injection time being kept constant and the flow reduced by half, the volume of the contrast material bolus was reduced by half in group A: 35 mL in patients <80 kg and 0.5 mL/kg in patients >80 kg, maximum 45 mL. Group B patients underwent a standard coronary CTA injection protocol, consisting of a contrast material bolus injected at 5 mL/s (iodine rate =2 g/s) into an 18G catheter, followed by a 20 mL saline rinse at the same rate. The volume of the bolus was determined according to the weight of the patient: 70 mL for patients <80 kg and 1 mL/kg for patients >80 kg, to a maximum of 90 mL.

Image acquisition

All examinations were performed on a commercially

available dual-layer spectral CT (IQon spectral CT; Philips Healthcare). This novel scanner acquires spectral data per default at each CT scan. Patients were placed in supine position, arms above the head. If necessary, patients received intravenous beta-blocker (esmolol chlorohydrate, Esmocard; Orpha Devel Handels Vertriebs GMBH, Austria) to reach a pre-scan heart rate of ≤65 bpm. Unless contraindicated, sublingual spray of nitroglycerin (Natispray; Teofarma SRL, Italy) was administered to all patients.

Retrospective ECG-gating was used for the acquisition of the arterial phase. The detailed scanning parameters were: tube potential: 120 kVp; tube current: 220 mAs; gantry revolution time: 0.27s; automatic exposure control (angular and longitudinal), combined xyz axis; detector collimation: 64 mm × 0.625 mm, scanning field of view: 22 cm. Bolus tracking was used, with a region of interest (ROI) placed in the descending aorta and a cut-off value of 130 HU.

Image reconstruction

Data acquired with both injection protocols were reconstructed with the same parameters, the dedicated reconstructions that are employed in clinical practice to assess the left ventricle myocardium. Data were reconstructed at a specific targeted mid-diastolic phase (78%) of the R-R interval with a large field-of-view (FOV) of 500 mm, a slice thickness of 3 mm (increment 1.5 mm) and a soft kernel (CB, cardiac routine). The same iterative reconstruction strength was employed (iDose 3).

Image segmentation and analysis

Regions of interest were drawn manually in the 16 myocardial segments according to the American Heart Association recommendations (apex excluded) by a radiologist specialized in cardiac imaging (SB, 7 years of experience) on multiplanar reconstructions of the heart in short axis planes (*Figure 2*). Abnormal segments, for instance due to motion artefacts, were excluded. The subendocardial and epicardial regions and coronary arteries were avoided. Circular ROIs were drawn in the lumen of the left ventricular cavity at basal, mid and apical level as well as in homogeneous areas of the paravertebral and intercostal muscles. Mean values and standard deviation were recorded for each of the reconstructed series (conventional images, iodine maps and VMI).

VMI between 40 and 70 keV in 10 keV increments were reconstructed and analysed (*Figure 2*). These reconstructions were chosen considering that the peak of iodine attenuation is at low energy (<40 keV), 40 keV is the lowest possible value for reconstruction of VMI and images of 74–75 keV are equivalent of conventional images at 120 kVp. Therefore, all VMI images with energy values in-between are expected to present higher attenuation values as compared to conventional images in voxels containing iodine (19).

A quantitative assessment of iodine concentration (in mg/mL) in each myocardial segment was performed using the dedicated software package (Spectral IntelliSpace Portal, ISP) on the iodine maps generated with a two material-based (iodine-water) decomposition (*Figure 2*).

VMI and iodine maps were generated by the dedicated and proprietary software IntelliSpace Portal (Philips Healthcare, Best, the Netherlands) based on the model of Alvarez and Mackowsky and material decomposition (20). Thanks to this software, all spectral images can be reconstructed at any time during postprocessing starting from a specific dataset created by the CT scanner after acquisition. Inside the dedicated interface, it is also possible to switch between conventional and spectral images on a user-predefined plane, which is how we proceeded for this study.

Iodine concentration

Average iodine concentration of the 16 segments in the two groups was compared. For each group, iodine concentrations in each of the 16 segments, in basal, mid and apical segments (basal segments: 1, 2, 3, 4, 5, 6; mid segments: 7, 8, 9, 10, 11, 12; apical segments: 13, 14, 15, 16) as well as in three regions defined as anteroseptal-anterior (corresponding to segments: 1, 2, 7, 8, 13, 14), inferoseptal-inferior (corresponding to segments: 3, 4, 9, 10, 15) and lateral (corresponding to segments: 5, 6, 11, 12, 16) were compared.

The same comparisons were repeated for iodine values of myocardial segments normalised for the iodine concentration of the left ventricle at the corresponding level. The following formula was used: iodine concentration of a myocardial segment/iodine concentration in the cavity of the left ventricle on the corresponding plane.

Objective quality analysis

Image noise, SNR and CNR between the myocardial segments and paravertebral muscle were measured using the

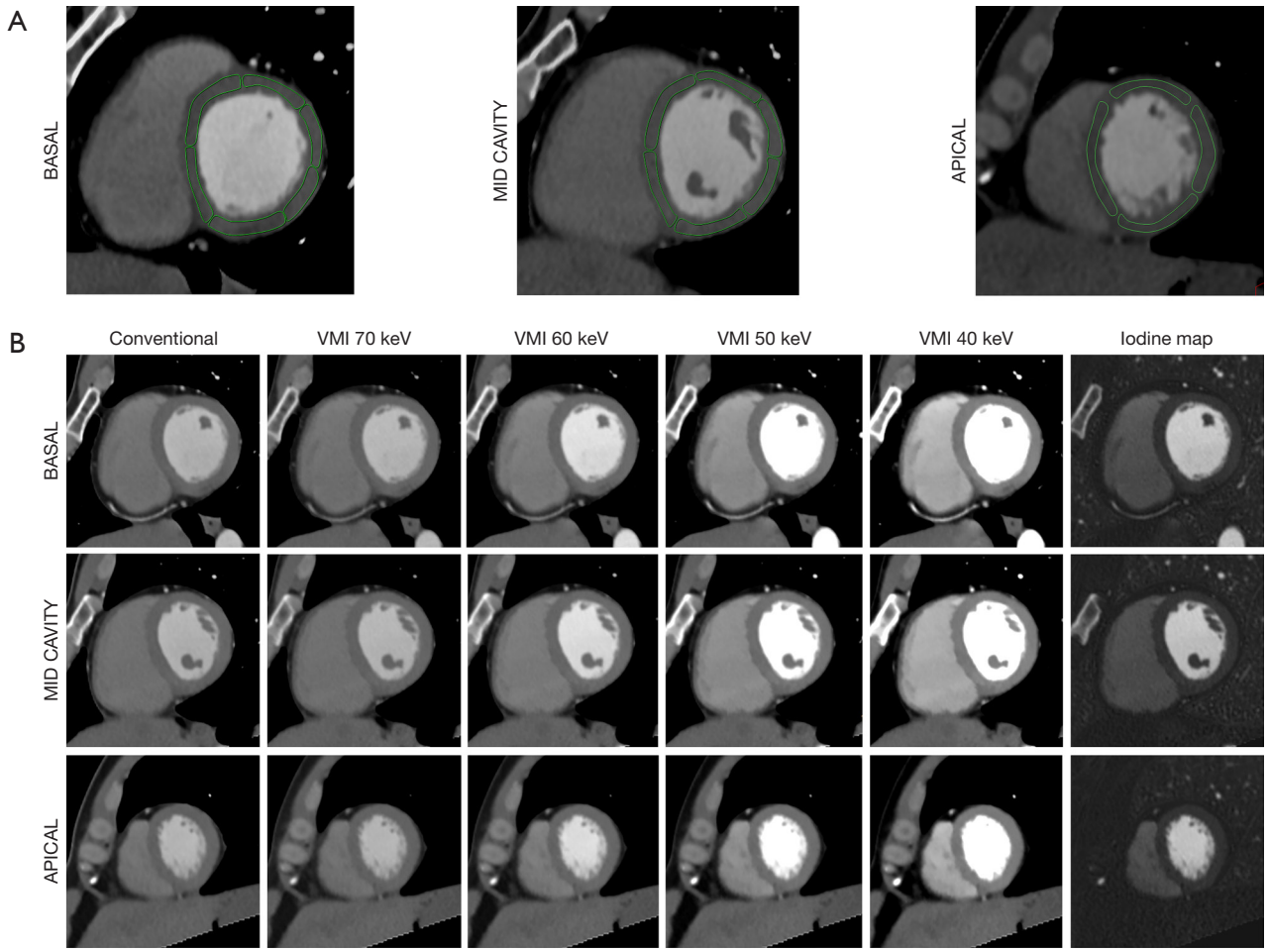

Figure 2 Myocardial segmentation and assessed spectral images. (A) Example of myocardial segmentation into 16 segments according to the AHA recommendation. At first, short axis images at basal, mid cavity and apical level were manually obtained on a workstation allowing for multiplanar reconstructions. Then, the contours of the AHA segments were manually drawn (as shown in green in this figure). (B) Display of all assessed spectral images (conventional, VMI 70-60-50-40 keV and iodine maps) in a case example of first pass myocardial perfusion for protocol A (rate at 2.5 mL/s). AHA, American Heart Association; VMI, virtual monochromatic images.

ROIs measurement on the conventional and VMI images as follows:

$$Image\ noise = \frac{SD\ myocardial + SD\ paravertebral\ muscle}{2} \quad [1]$$

$$SNR = \frac{Mean\ value}{Standard\ deviation}\ for\ each\ ROI \quad [2]$$

$$CNR = \frac{Mean\ value\ myocardial - mean\ value\ paravertebral\ muscle}{\left(\frac{SD\ myocardial + SD\ paravertebral\ muscle}{2}\right)} \quad [3]$$

Average image noise, SNR and CNR values of each myocardium were compared between conventional images and the four monochromatic reconstructions for the two groups.

Statistical analysis

All statistical analyses were performed with R (R v. 3.4.3, R Foundation for Statistical Computing, Vienna, Austria). Continuous values were presented as mean ± standard deviation (SD) or as median with interquartile ranges (IQR). Student's *t*-test and Wilcoxon were employed to compare patients' characteristics. Wilcoxon Mann Whitney and Kruskal-Wallis were employed for comparison between

Table 1 Characteristics of the 60 patients

Criteria	Group A (n=30)	Group B (n=30)	P value
Age (years)	50.1±17.3 (18–77)	50.8±18 (22–80)	0.87
Gender (men)	19 (63%)	20 (67%)	0.8
Weight (kg)	68 (22.3)	73.5 (24)	0.08
Height (cm)	170±10.1 (153–198)	170±9.7 (152–186)	0.96
BMI (kg/m^2)	23.9 (5.2)	25.8 (6.8)	0.05
HR (bpm)	69±10 (52–85)	67.8±11.2 (53–88)	0.69
Dose (CTDI mGy)	17.5 (10.9)	22.7 (15.8)	0.06

Data are presented as mean ± standard deviation (range) or median (IQ range). BMI, body mass index; CTDI, computed tomography dose index; HR, heart rate.

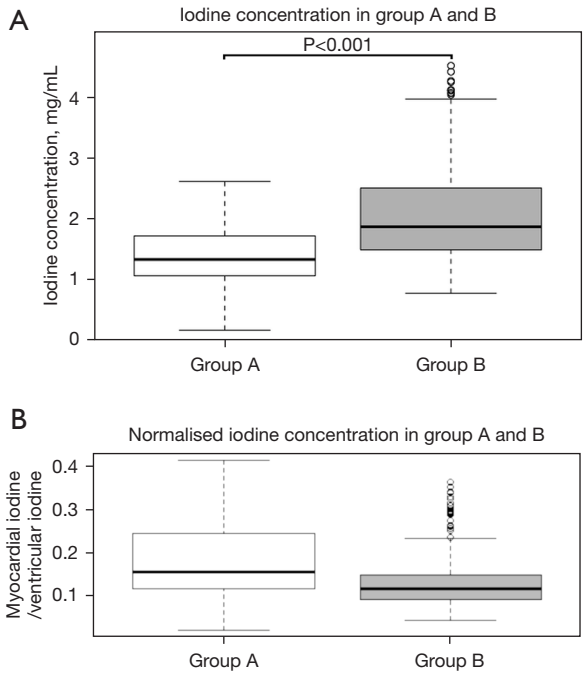

Figure 3 Box plots of absolute and normalised iodine concentrations in the two groups. (A) Box plots of overall myocardial iodine concentrations measured in the two protocols (group A: 2.5 mL/s; group B: 5 mL/s) for absolute values. (B) Box plots of normalised myocardial iodine measured in the two protocols. The difference between the two groups was statistically significant with higher values in group B. The opposite is true for normalised values that were significantly higher in group A, due to the higher iodine concentration in the cavity of the left ventricle.

different myocardial segments, territories and protocols. Missing data were excluded pairwise. The pairwise Wilcoxon test with Bonferroni correction was used for comparison between groups and post hoc analysis. Values of P<0.05 were considered statistically significant.

Results

Population

A total of 60 patients were analysed, of whom 30 underwent reduced injection protocol due to bad venous access (group A) and 30 protocol B (group B). The characteristics of the 60 patients are shown in *Table 1*. The comparison of the two patient groups did not reveal any significant differences in age, gender, heart rate, weight and height, body mass index (BMI) and radiation dose. All patients were administered nitroglycerin prior to the coronary-CTA.

Due to motion artefacts, 1 segment out of 480 (0.2%) and 7 segments out of 480 (1.5%) were excluded from analysis in group A and B respectively.

Iodine density maps

The mean iodine concentration values in myocardial segments vascularised by coronary arteries without significant stenosis were 1.38±0.41 mg/mL (range, 0.6–2.24 mg/mL; median: 1.33 mg/mL; IQR: 0.66 mg/mL) for protocol A and 2.07±0.73 mg/mL (range, 1.17–3.94 mg/mL; median: 1.87 mg/mL; IQR: 1.02 mg/mL) for protocol B (*Figure 3*), corresponding to a significant difference (P<0.001). For normalised values the difference was also significant (P<0.001) but with higher values in group A (median: 1.54, IQR: 0.13 for group A; median 0.12, IQR: 0.06 for group B) (*Figure 3*).

Iodine concentration values of the 16 segments, of basal, mid and apical segments and in the three wall regions are shown in *Table 2*.

Table 2 Iodine concentration values

Iodine concentration	Group A		Group B		Absolute A *vs.* absolute B
	Absolute	Normalised values	Absolute	Normalised values	
Total	1.33 (0.62)	0.15 (0.13)	1.87 (1.02)	0.12 (0.06)	<0.001
Segments					
Segment 1	1.32 (0.53)	0.14 (0.10)	1.92 (0.76)	0.12 (0.05)	<0.001
Segment 2	1.34 (0.79)	0.15 (0.12)	1.86 (0.95)	0.11 (0.05)	0.003
Segment 3	1.34 (0.68)	0.15 (0.13)	2.02 (0.73)	0.12 (0.05)	<0.001
Segment 4	1.16 (0.47)	0.14 (0.09)	1.62 (1.07)	0.10 (0.06)	<0.001
Segment 5	1.41 (0.58)	0.17 (0.11)	2.15 (1)	0.12 (0.05)	<0.001
Segment 6	1.46 (0.55)	0.17 (0.12)	2.2 (1.05)	0.13 (0.05)	<0.001
Segment 7	1.26 (0.62)	0.14 (0.14)	1.71 (0.98)	0.11 (0.07)	<0.001
Segment 8	1.39 (0.73)	0.16 (0.14)	1.69 (1.15)	0.12 (0.06)	0.002
Segment 9	1.25 (0.74)	0.13 (0.13)	1.77 (1)	0.11 (0.07)	<0.001
Segment 10	1.28 (0.72)	0.15 (0.12)	1.79 (1.26)	0.10 (0.07)	<0.001
Segment 11	1.44 (0.5)	0.17 (0.13)	1.95 (0.8)	0.13 (0.06)	<0.001
Segment 12	1.41 (0.52)	0.16 (0.11)	2.06 (0.9)	0.12 (0.06)	<0.001
Segment 13	1.25 (0.59)	0.14 (0.13)	1.57 (0.91)	0.10 (0.04)	0.001
Segment 14	1.37 (086)	0.16 (0.15)	1.68 (1.08)	0.11 (0.06)	0.003
Segment 15	1.27 (0.58)	0.15 (0.13)	1.66 (1.03)	0.11 (0.04)	<0.001
Segment 16	1.34 (0.57)	0.16 (0.13)	1.78 (0.91)	0.12 (0.03)	<0.001
Basal, mid, apical					
Basal	1.33 (0.65)	0.15 (0.12)	1.99 (0.99)	0.12 (0.06)	<0.001
Mid	1.36 (0.63)	0.16 (0.13)	1.88 (1.06)	0.11 (0.07)	<0.001
Apical	1.31 (0.61)	0.15 (0.13)	1.66 (1.04)	0.11 (0.05)	<0.001
Wall regions					
Anteroseptal-anterior	1.32 (0.68)	0.15 (0.13)	1.72 (1.05)	0.11 (0.06)	<0.001
Inferoseptal-inferior	1.25 (0.22)	0.14 (0.12)	1.74 (0.28)	0.11 (0.06)	<0.001
Lateral	1.41 (0.24)	0.16 (0.12)	2.07 (0.04)	0.12 (0.05)	<0.001

Data regarding iodine concentration (mg/mL) are presented as: median (interquartile range).

A sub-analysis comparing iodine concentration in the 16 segments showed no significant difference for both protocols (P=0.47 and P=0.09 for iodine concentrations; P=0.81 and P=0.26 for normalised values in protocol A and B respectively). The segments showing the lowest values were segment 4 in group A (median: 1.16; IQR: 0.47) and segments 13 (median: 1.57; IQR: 0.91) and 4 in group B (median: 1.62; IQR: 1.07) (*Figure 4*).

In both groups no statistically significant difference was found between basal, mid-ventricular and apical segments (P=0.28 and P=0.12 for iodine concentrations; P=0.67 and P=0.38 for normalised values respectively for protocol A and B). Significant differences were found for both groups between different wall regions (P=0.04 and P<0.001 for group A and B) (*Figure 4*). However, in group A analysis of normalised data (P=0.06) did not show significant differences

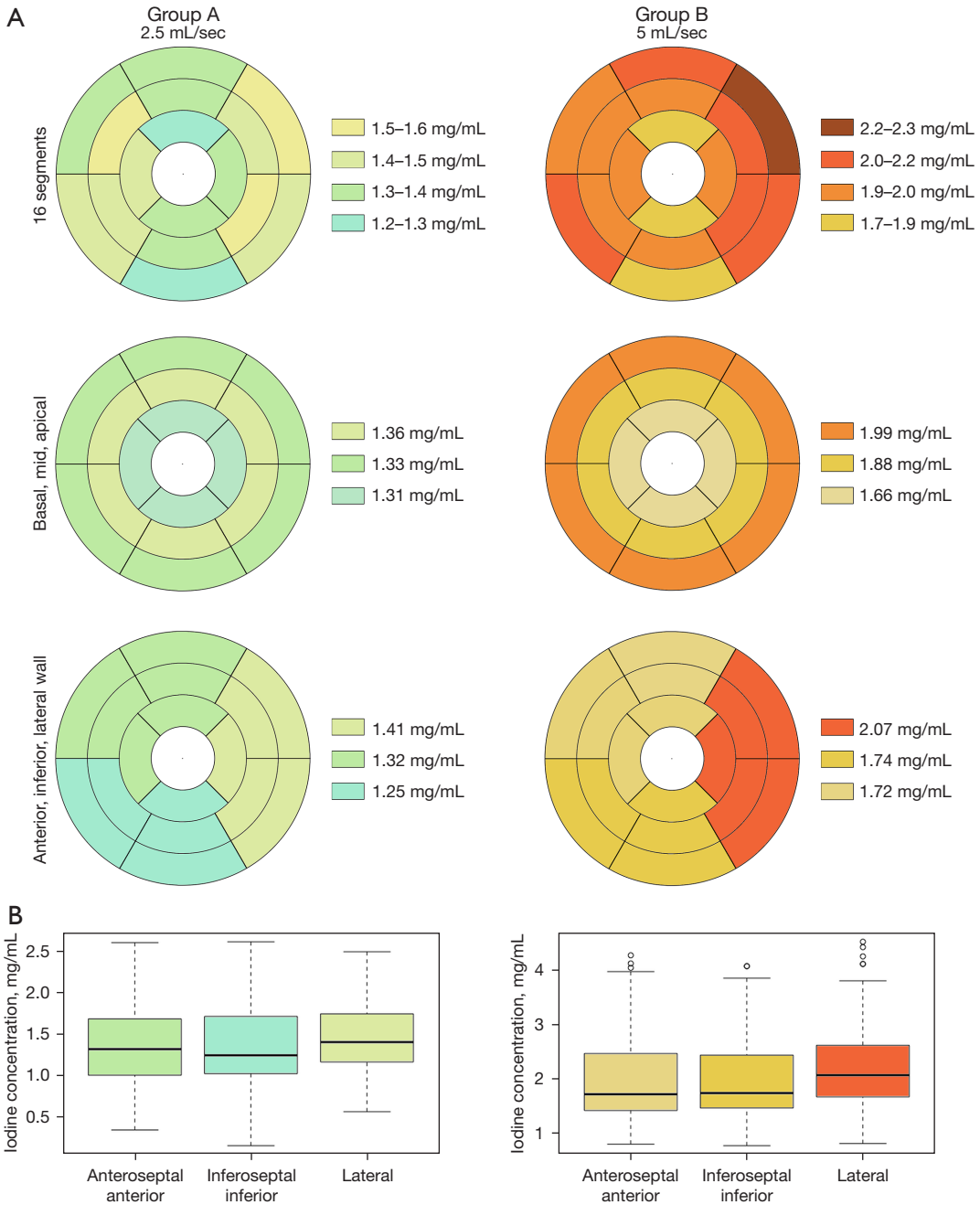

Figure 4 Visual representation of iodine density in the different analysed regions in the two groups. (A) Display of color-coded iodine density in the 16 segments, basal, mid and apical segments and anterior, inferior and lateral wall regions in the two groups. Color-coding is illustrated in the legend next to each bull's eye graph. (B) Box plots of the iodine concentrations measured in the 3 different wall regions for the two protocols. To be noticed that the range of values of the y-axis is different for the two groups.

between wall regions. In group B the lateral territory showed the highest values (median: 2.07 mg/mL; IQR: 0.4) and was significantly different from the anteroseptal-anterior (median: 1.72; IQR: 1.04) and inferoseptal-inferior (median: 1.74; IQR: 0.8) territories (P<0.01 for both absolute and normalised values) (*Figures 4,5*).

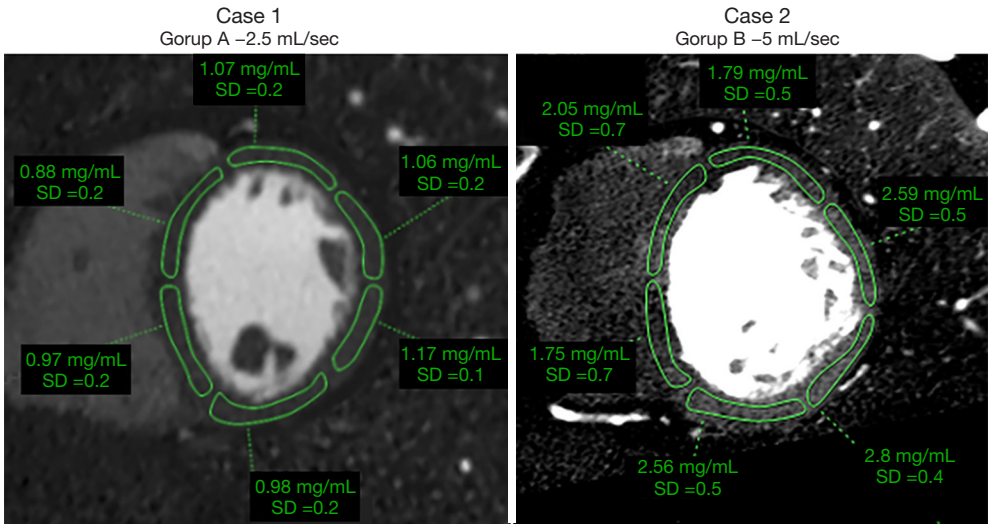

Figure 5 On the left, iodine map of one case from the group with low dose and slow injection rate shows a homogeneous myocardium on this short axis reconstruction at mid cavity. On the contrary, on the right a case example from the group with high dose at high injection rate demonstrates a heterogeneous myocardium with a higher iodine density in the lateral wall, as highlighted by the measurements provided for each of the mid-cavity segments.

Objective quality

The values of noise, SNR and CNR for conventional images and VMI are displayed in *Table 3* and *Figure 6*.

Image noise

Noise values showed significant differences in multiple group testing (P<0.01). In group A post-hoc analysis showed significant differences for 70 *vs.* 50 keV and between 40 keV and all other reconstructions (P=0.05). In group B differences were significant for conventional *vs.* 70 keV, 50 *vs.* 70 and 60 keV as well as 40 keV and all other reconstructions (P=0.05).

Signal to noise ratio

SNR presented significant differences in multiple groups testing for both injection protocols (P<0.01). Post-hoc testing revealed significant results in the following groups: conventional *vs.* 60 keV, conventional *vs.* 50 keV, conventional *vs.* 40 keV for protocol A and between conventional and all VMI for protocol B.

Contrast to noise ratio

The CNR values were significantly different in multiple groups testing in both groups (P<0.01). In group A, post-hoc testing found significant differences for all associations except for conventional *vs.* 70 keV. In group B, differences were not significant for groups conventional *vs.* 70 keV, 70 *vs.* 60 keV, 60 *vs.* 50 keV, 50 *vs.* 40 keV.

Differences of noise, CNR and SNR between the two groups

CNR and noise values presented significant differences between corresponding reconstructions of the two groups, except for CNR at 40 keV and noise at 70 keV, with higher values for group B. SNR did not show significant differences between corresponding reconstructions in the two groups (*Table 3*, *Figure 6*).

Discussion

The present study demonstrated a significant difference in left ventricular myocardium iodine concentration between two groups of patients, both without significant coronary arteries stenosis, undergoing different injection protocols with higher values in the higher flow rate and iodine load cohort. In both groups, iodine concentration was not significantly different between the 16 segments, as well as in basal, mid and apical territories. In both groups significant differences between wall regions were found although more

Table 3 Noise, SNR and CNR values

	Conventional			VMI											
				70 keV			60 keV			50 keV			40 keV		
	A	B	P value	A	B	P value	A	B	P value	A	B	P value	A	B	P value
Noise			<0.01			0.04			0.01			0.01			0.01
Median	0.83	2.11		0.43	1.32		0.85	2.46		1.28	3.72		2.28	6.15	
IQR	1.66	2.16		1.19	2.17		1.34	2.53		2.58	2.98		3.65	4.28	
SNR			0.64			0.83			0.8			0.55			0.26
Median	7.48	6.95		9.22	9.00		9.91	8.92		10.31	9.48		10.84	9.34	
IQR	3.10	2.78		3.96	3.73		3.65	3.89		4.31	3.90		4.71	3.89	
CNR			0.047			0.01			0.01			0.02			0.08
Median	2.55	3.32		2.96	4.15		4.14	5.64		5.73	7.27		7.35	8.67	
IQR	−0.89	−1.16		−1.77	−1.98		−2.80	−3.12		−3.15	−4.29		−3.70	−4.39	

CNR, contrast to noise ratio; SNR, signal to noise ratio; VMI, virtual monochromatic image.

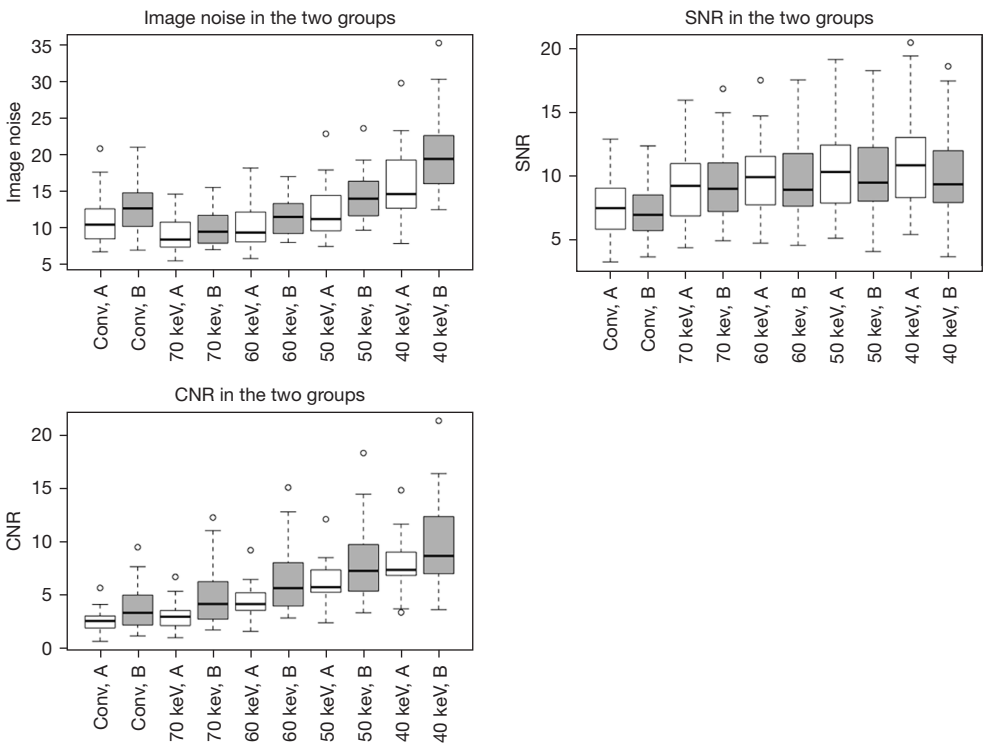

Figure 6 Box plots of image noise, SNR and CNR ratios measured with the conventional and mono-energetic images (70, 60, 50, 40 keV) for the two protocols (A =2.5 mL/s in white; B =5 mL/s in grey). SNR, signal to noise ratio; CNR, contrast to noise ratio.

pronounced in the higher flow rate group. This difference among territories was confirmed on normalised iodine values only for the group with higher flow rate and iodine load. CNR and SNR but also image noise showed gradually increasing values as keV values decreased.

We found an iodine concentration of 1.38±0.41 mg/mL for group A and 2.07±0.73 mg/mL for group B with lowest values of 0.6 and 1.17 mg/mL respectively. Previous studies demonstrated that iodine concentration can reliably be quantified even for values as low as 0.5 or 1 mg/mL in 20 cm or 30 cm × 40 cm phantoms, respectively, and with minimum detectable differences of 0.4 mg/mL (21-24). Thus, both proposed protocols can be employed in clinical practice for both myocardial and coronary assessment. Indeed, a study carried out on the same population demonstrated the non-inferiority of the low rate injection protocol for coronary artery assessment (18). Nevertheless, the injection protocol with higher rate might provide more accurate calculations of iodine concentrations as different studies have shown an increase in accuracy for higher iodine concentrations (15,17).

The results of our study showed that myocardial iodine concentration as assessed with DE-DLCT differs according to contrast injection protocol. Iodine concentration has been regarded as a surrogate of myocardial perfusion and its objective quantification as a potentially helpful tool not only for the detection of focal perfusion defects but also for the determination of global perfusion reduction in three vessel disease (10,11,13,14). Different studies aimed at establishing a precise threshold value of iodine concentration to distinguish normal, ischemic and necrotic myocardium based on DECT acquisitions (13,14). Delgado *et al.* found that a cut-off value of 2.1 mg/mL had a sensitivity of 75 % and a specificity of 73.6 % to differentiate normal from hypoperfused territories on stress exams (13). Distinction between ischemic and necrotic segments was not possible due to overlap between iodine values. van Assen *et al.* found optimal values of 2.5 mg/mL at rest and 2.1 mg/mL during stress for distinction of healthy and diseased segments(14). Only at rest a threshold value could be defined to distinguish ischemic from necrotic territories corresponding to 1.00 mg/mL, with a sensitivity of 80% and a specificity of 100%. However, in these studies all scans were performed under the same injection conditions. On the contrary, our study demonstrates that fist-pass myocardial perfusion is a function of injection protocols. Therefore, an absolute threshold might be more challenging to define and should definitely take into account injection parameters as well as left ventricle iodine content.

Furthermore, we showed that injection parameters influence iodine concentration homogeneity in different wall regions of the myocardium. Indeed, we found significant differences in iodine concentrations between wall regions. Although clearly demonstrated in the high flow and high iodine load group, this difference was doubtful in the low flow and low dose group. To the best of our knowledge this is the first study assessing myocardium homogeneity in the absence of significant coronary stenosis with DE-DLCT. However, other studies demonstrated myocardial heterogeneity in healthy volunteers with different imaging techniques (25-27). Kim *et al.* found perfusion differences between segments as high as 32% at rest and 28% during stress with the septum showing lower values, although the difference was not statistically significant (26). Similarly to our results, Ho *et al.* demonstrated higher perfusion values in the lateral wall of low risk patients both at rest and under stress (25). Whether the differences we observed could have an impact on detectability of hypoperfusion areas in patients with coronaropathy still has to be investigated. Nevertheless, it should be kept in mind that higher injection rates and contrast dose influence iodine distribution homogeneity in subjects without underlying significant coronary artery stenosis.

Although not statistically significant in either of the two groups, some of the 16 segments showed lower iodine concentrations. The lowest values were found in segments 4 and 13 for protocol B. Segmental HU values lower than remote myocardium have been previously described and have been referred mainly to beam hardening artefacts (7,28,29). Our findings suggest that also iodine maps are affected by these artefacts, as we found lower than average values of iodine concentration in the same segments.

Virtual monoenergetic reconstructions have been considered of particular interest in cardiovascular imaging. As the peak of mass attenuation coefficient for iodine can be found at low energy levels, the attenuation value of iodinated contrast material is higher on monoenergetic images at lower keV (5,8). Accordingly, we found that both SNR and CNR increased as the energetic value of the reconstruction decreased with the highest values at 40 keV. Nevertheless, image noise showed the opposite pattern increasing as the energetic value of the reconstruction decreased. Therefore, the optimal images for clinical evaluation are most likely not found at lowest values but around 50 keV. Furthermore, both CNR and image noise were significantly higher in group B without

corresponding increase of SNR. Further studies are needed to confirm if the combination of first-pass DE-DLCT myocardial perfusion with low flow rate and iodine load and assessment on iodine maps and low energy monoenergetic reconstructions will improve the detection of hemodynamic significant stenosis.

The first limitation of our study is the lack of a standard of reference for both iodine quantification and its homogeneity. Therefore, not only the accuracy of absolute values but also the presence relative regional differences could not be confirmed. As a consequence, the influence and impact of artefacts (beam hardening but not only) could not be distinguished from intrinsic perfusion variability. Secondly, we investigated only two injection protocols that differed in both injection rate and contrast media volume. Although the differences we found are more probably related to the different injection rate, we cannot exclude an influence of other parameters. The two injection rates were quite apart from each other and it is likely the best protocol being in-between. Thirdly, another limitation to the current study is the lack of data about inter-observer variability. Indeed, segmentation was performed by an experienced, albeit single, observer. Furthermore, due to the retrospective nature of this study, the two groups differed for one parameter, that is the status of the veins accessible for injection. As specified above, this was in fact the parameter that prompted the clinicians to prefer one injection protocol over the other as commonly done in clinical practice. Although, to the best of our knowledge, there is no report of a connection between the status of veins and first pass myocardial perfusion, we cannot completely rule out some influence of this factor on our results. Further prospective studies will have to ascertain if veins status can influence by itself first pass myocardial perfusion. Nevertheless, the most important message of the present study, the fact that first pass perfusion is a complex function and that generalized absolute iodine concentration thresholds should be avoided, remains valuable and unchanged.

To conclude, we demonstrated that injection protocols influence first pass myocardial iodine concentration. At higher flow rates, left ventricular myocardium presents higher iodine concentration and presents different iodine concentrations in the anterior, inferior and lateral myocardial regions even in the absence of significant coronary stenosis. Both factors should be considered when assessing the presence of perfusion defects both subjectively and quantitatively.

Acknowledgments

Funding: None.

Footnote

Reporting Checklist: The authors have completed the STROBE reporting checklist. Available at https://qims.amegroups.com/article/view/10.21037/qims-21-809/rc

Conflicts of Interest: All authors have completed the ICMJE uniform disclosure form (available at https://qims.amegroups.com/article/view/10.21037/qims-21-809/coif). The authors have no conflicts of interest to declare.
Ethical Statement: The authors are accountable for all aspects of the work in ensuring that questions related to the accuracy or integrity of any part of the work are appropriately investigated and resolved. The study was conducted in accordance with the Declaration of Helsinki (as revised in 2013). The study was approved by the local ethics committee (No. 19-382) and informed consent was waived due to the retrospective nature of the study.

References

1. Tonino PA, Fearon WF, De Bruyne B, Oldroyd KG, Leesar MA, Ver Lee PN, Maccarthy PA, Van't Veer M, Pijls NH. Angiographic versus functional severity of coronary artery stenoses in the FAME study fractional flow reserve versus angiography in multivessel evaluation. J Am Coll Cardiol 2010;55:2816-21.
2. Tonino PA, De Bruyne B, Pijls NH, Siebert U, Ikeno F, van' t Veer M, Klauss V, Manoharan G, Engstrøm T, Oldroyd KG, Ver Lee PN, MacCarthy PA, Fearon WF; FAME Study Investigators. Fractional flow reserve

versus angiography for guiding percutaneous coronary intervention. N Engl J Med 2009;360:213-24.
3. Takx RA, Blomberg BA, El Aidi H, Habets J, de Jong PA, Nagel E, Hoffmann U, Leiner T. Diagnostic accuracy of stress myocardial perfusion imaging compared to invasive coronary angiography with fractional flow reserve meta-analysis. Circ Cardiovasc Imaging 2015;8:e002666.
4. Rossi A, Merkus D, Klotz E, Mollet N, de Feyter PJ, Krestin GP. Stress myocardial perfusion: imaging with multidetector CT. Radiology 2014;270:25-46.
5. Johnson TR. Dual-energy CT: general principles. AJR Am J Roentgenol 2012;199:S3-8.
6. McCollough CH, Leng S, Yu L, Fletcher JG. Dual- and Multi-Energy CT: Principles, Technical Approaches, and Clinical Applications. Radiology 2015;276:637-53.
7. So A, Hsieh J, Narayanan S, Thibault JB, Imai Y, Dutta S, Leipsic J, Min J, LaBounty T, Lee TY. Dual-energy CT and its potential use for quantitative myocardial CT perfusion. J Cardiovasc Comput Tomogr 2012;6:308-17.
8. Vlahos I, Chung R, Nair A, Morgan R. Dual-energy CT: vascular applications. AJR Am J Roentgenol 2012;199:S87-97.
9. Scheske JA, O'Brien JM, Earls JP, Min JK, LaBounty TM, Cury RC, Lee TY, So A, Hague CJ, Al-Hassan D, Kuriyabashi S, Dowe DA, Leipsic JA. Coronary artery imaging with single-source rapid kilovolt peak-switching dual-energy CT. Radiology 2013;268:702-9.
10. Ko SM, Choi JW, Song MG, Shin JK, Chee HK, Chung HW, Kim DH. Myocardial perfusion imaging using adenosine-induced stress dual-energy computed tomography of the heart: comparison with cardiac magnetic resonance imaging and conventional coronary angiography. Eur Radiol 2011;21:26-35.
11. Wang R, Yu W, Wang Y, He Y, Yang L, Bi T, Jiao J, Wang Q, Chi L, Yu Y, Zhang Z. Incremental value of dual-energy CT to coronary CT angiography for the detection of significant coronary stenosis: comparison with quantitative coronary angiography and single photon emission computed tomography. Int J Cardiovasc Imaging 2011;27:647-56.
12. Ruzsics B, Schwarz F, Schoepf UJ, Lee YS, Bastarrika G, Chiaramida SA, Costello P, Zwerner PL. Comparison of dual-energy computed tomography of the heart with single photon emission computed tomography for assessment of coronary artery stenosis and of the myocardial blood supply. Am J Cardiol 2009;104:318-26.
13. Delgado Sánchez-Gracián C, Oca Pernas R, Trinidad López C, Santos Armentia E, Vaamonde Liste A, Vázquez Caamaño M, Tardáguila de la Fuente G. Quantitative myocardial perfusion with stress dual-energy CT: iodine concentration differences between normal and ischemic or necrotic myocardium. Initial experience. Eur Radiol 2016;26:3199-207.
14. van Assen M, Lavra F, Schoepf UJ, Jacobs BE, Williams BT, Thompson ZM, Varga-Szemes A, Ruzsics B, Oudkerk M, Vliegenthart R, De Cecco CN. Iodine quantification based on rest / stress perfusion dual energy CT to differentiate ischemic, infarcted and normal myocardium. Eur J Radiol 2019;112:136-43.
15. Sauter AP, Kopp FK, Münzel D, Dangelmaier J, Renz M, Renger B, Braren R, Fingerle AA, Rummeny EJ, Noël PB. Accuracy of iodine quantification in dual-layer spectral CT: Influence of iterative reconstruction, patient habitus and tube parameters. Eur J Radiol 2018;102:83-8.
16. van Hamersvelt RW, Willemink MJ, de Jong PA, Milles J, Vlassenbroek A, Schilham AMR, Leiner T. Feasibility and accuracy of dual-layer spectral detector computed tomography for quantification of gadolinium: a phantom study. Eur Radiol 2017;27:3677-86.
17. Pelgrim GJ, van Hamersvelt RW, Willemink MJ, Schmidt BT, Flohr T, Schilham A, Milles J, Oudkerk M, Leiner T, Vliegenthart R. Accuracy of iodine quantification using dual energy CT in latest generation dual source and dual layer CT. Eur Radiol 2017;27:3904-12.
18. Rotzinger DC, Si-Mohamed SA, Yerly J, Boccalini S, Becce F, Boussel L, Meuli RA, Qanadli SD, Douek PC. Reduced-iodine-dose dual-energy coronary CT angiography: qualitative and quantitative comparison between virtual monochromatic and polychromatic CT images. Eur Radiol 2021;31:7132-42.
19. Adam SZ, Rabinowich A, Kessner R, Blachar A. Spectral CT of the abdomen: Where are we now? Insights Imaging 2021;12:138.
20. Rassouli N, Etesami M, Dhanantwari A, Rajiah P. Detector-based spectral CT with a novel dual-layer technology: principles and applications. Insights Imaging 2017;8:589-98.
21. Li Y, Shi G, Wang S, Wang S, Wu R. Iodine quantification with dual-energy CT: phantom study and preliminary experience with VX2 residual tumour in rabbits after radiofrequency ablation. Br J Radiol 2013;86:20130143.
22. Sellerer T, Noël PB, Patino M, Parakh A, Ehn S, Zeiter S, Holz JA, Hammel J, Fingerle AA, Pfeiffer F, Maintz D, Rummeny EJ, Muenzel D, Sahani DV. Dual-energy CT: a phantom comparison of different platforms for abdominal imaging. Eur Radiol 2018;28:2745-55.

23. Euler A, Solomon J, Mazurowski MA, Samei E, Nelson RC. How accurate and precise are CT based measurements of iodine concentration? A comparison of the minimum detectable concentration difference among single source and dual source dual energy CT in a phantom study. Eur Radiol 2019;29:2069-78.
24. Jacobsen MC, Cressman ENK, Tamm EP, Baluya DL, Duan X, Cody DD, Schellingerhout D, Layman RR. Dual-Energy CT: Lower Limits of Iodine Detection and Quantification. Radiology 2019;292:414-9.
25. Ho KT, Ong HY, Tan G, Yong QW. Dynamic CT myocardial perfusion measurements of resting and hyperaemic blood flow in low-risk subjects with 128-slice dual-source CT. Eur Heart J Cardiovasc Imaging 2015;16:300-6.
26. Kim EY, Chung WJ, Sung YM, Byun SS, Park JH, Kim JH, Moon J. Normal range and regional heterogeneity of myocardial perfusion in healthy human myocardium: assessment on dynamic perfusion CT using 128-slice dual-source CT. Int J Cardiovasc Imaging 2014;30 Suppl 1:33-40.
27. Chareonthaitawee P, Kaufmann PA, Rimoldi O, Camici PG. Heterogeneity of resting and hyperemic myocardial blood flow in healthy humans. Cardiovasc Res 2001;50:151-61.
28. Rodríguez-Granillo GA, Rosales MA, Degrossi E, Rodriguez AE. Signal density of left ventricular myocardial segments and impact of beam hardening artifact: implications for myocardial perfusion assessment by multidetector CT coronary angiography. Int J Cardiovasc Imaging 2010;26:345-54.
29. Ko SM, Choi JW, Hwang HK, Song MG, Shin JK, Chee HK. Diagnostic performance of combined noninvasive anatomic and functional assessment with dual-source CT and adenosine-induced stress dual-energy CT for detection of significant coronary stenosis. AJR Am J Roentgenol 2012;198:512-20.

Cite this article as: Boccalini S, Si-Mohamed S, Matzuzzi M, Tillier M, Rotzinger DC, Revel D, Boussel L, Douek P. Effect of contrast material injection protocol on first-pass myocardial perfusion assessed by dual-energy dual-layer computed tomography. Quant Imaging Med Surg 2022. doi: 10.21037/qims-21-809